Solar Energy 215 (2021) 482–491

Contents lists available at ScienceDirect

Solar Energy

journal homepage: www.elsevier.com/locate/solener

Improved field evaluation of reference cells using spectral measurements

Frank Vignola [a,*], Josh Peterson [a], Richard Kessler [a], Vikram Sandhu [a], Sean Snider [b], Aron Habte [c], Peter Gotseff [c], Afshin Andreas [c], Manajit Sengupta [c], Fotis Mavromatakis [d]

[a] University of Oregon, Eugene, OR 97403, USA
[b] Saint Mary's High School, Medford, OR, USA
[c] National Renewable Energy Laboratory, Golden, CO 80301, USA
[d] Hellenic Mediterranean University, Herkalion, Crete, Greece

ARTICLE INFO

Keywords:
Reference solar cells
Spectral measurements
One-axis tracking
Pyranometer
Resource assessment

ABSTRACT

Output from an IMT reference solar cell mounted on a one-axis tracking surface is investigated using spectral measurements covering the 350–1650 nm range for selected days throughout the year. Comparisons are made to a Class-A pyranometer also mounted on the one-axis tracking surface. Systematic biases over the day and year are observed in the ratio of the reference cell's measurements to reference pyranometer measurements. This systematic bias is associated with the spectral, temperature, and angle-of-incident effects that differ between the reference cell and the reference pyranometer. The comparison is done for selected clear and totally cloudy days to determine the magnitude of the effects and to characterize the influence of these effects on the reference cell measurements. A model to calculate the reference cell output based on spectral irradiance and reference cell temperature is introduced.

1. Introduction

As larger photovoltaic (PV) plants come on line, there is a need to better understand, characterize, and forecast the electrical production from these facilities. Basic to these goals is an accurate measurement and understanding of the incident radiation. Comparisons between different PV system designs and technologies are dependent on accurate relative comparisons of incident radiation. Maintaining system performance is enhanced by measuring the changes in incident radiation from day to day. Three main sources of incident radiation come from databases derived from satellite images, ground-based measurements with high-quality broadband sensor, or co-located reference cells. High-quality ground-based measurements have been used to validate irradiance values derived from satellite images and to develop models to estimate total or global irradiance (GTI) on a PV module's surface. Broadband pyranometers have also been used to measure GTI for PV modules on tilted and tracking surfaces.

Reference cells, used on PV module assembly lines, are also used in the field to evaluate PV system performance. The advantage to using reference cells in the field is that they are constructed using the same the same solar cells, glazing, encapsulant, and backing as the PV module in the system they are monitoring. The main difference is that reference cells are designed to make short circuit current measurements while PV modules operate at the max power point to produce electricity. Reference cells can be placed in the plane-of-array of the PV modules and are used in the field because they have the equivalent spectral and cosine response of the PV modules deployed in the field (Habte et al., 2018). Pyranometers in the plane-of-array of PV modules are designed to measure the GTI on the modules. The measured irradiance data are used as inputs for software programs that estimate PV system performance. The estimated PV system performance can then be compared to actual system performance to ensure that the system is performing as expected. In addition, the measured incident irradiance can then be used to forecast the PV system production. Most models of PV system performance are based on high-quality Class-A pyranometer measurements. The use of reference cell measurements instead of high-quality irradiance measurements can introduce systematic biases into the estimated system performance or forecast.

The advantage of reference cells is that they incorporate spectral dependence and angle-of-incidence effects that influence PV module performance and these effects do not have to be modeled, as is necessary with pyranometer measurements. Since modeling introduces uncertainties, performance estimates using reference cells should result in smaller uncertainties (Meydbray et al., 2012). The disadvantage

* Corresponding author.
E-mail address: fev@uoregon.edu (F. Vignola).

https://doi.org/10.1016/j.solener.2020.12.063
Received 21 June 2020; Received in revised form 28 December 2020; Accepted 30 December 2020
Available online 24 January 2021

associated with reference cells is that they are not pyranometers and measurements at one angle and orientation cannot be used by standard models to translate the reference cell measured values to different tilts and orientations.

The initial goal of this study was to compare reference cell measurements with those from a high-quality pyranometer and to understand the differences between the measurements and look at the dependence of the comparison on the spectral distribution. This study is a culmination of several years of comparisons and provides ideas on where to make improvements in the next phase of reference cell studies (Vignola et al., 2017a, Vignola et al., 2017b, Vignola et al., 2018, Vignola et al., 2019). More specifically, while numerous comparisons were made with reference pyranometers, the systematic biases of pyranometers and reference cells make direct comparisons difficult and another approach is needed and suggested.

Before going into details and analysis of the work presented in this paper, a general discussion of reference cells is needed to establish the basic ideas. Reference cells are not pyranometers and when reference cells are compared to pyranometer measurements large biases are apparent. Three main sources of these reference cell biases are:

1. Spectral response of the reference cell
2. Temperature dependence
3. Deviation from an ideal cosine response

This study differs from many previous studies because spectral measurements are used to calculate the effect of changing spectral distributions over the day on the reference cell measurements. By using spectral measurements, the uncertainties associated with the modeled spectral distribution are eliminated. The experimental data used for this study comes from co-located spectral and reference cell instruments on a one-axis tracker located at the National Renewable Energy Laboratory's (NREL) Solar Radiation Research Laboratory (SRRL) in Golden, Colorado. Measurements made on a one-axis tracking surface minimizes, but does not eliminate the angle-of-incidence (AOI) effects.

This article is organized as follows:

- The experimental equipment and arrangement are described along with the uncertainty associated with measurements.
- Comparisons between reference solar cell measurements and reference Class-A pyranometer measurements are made for several clear sky days over the year.
- An analysis of the clear sky comparisons is then conducted. The effects for temperature and spectral radiation on the comparisons are then performed using reference cell temperature measurements and the measured spectral data.
- Comparisons under totally cloudy skies are then presented and evaluated.
- A simple model for calculating the reference cell output is presented and the results are compared with measured IMT reference cell measurements.
- The magnitude and nature of the differences between measured and modeled reference cell output are then discussed.
- Various characteristics of the uncertainties in the measurements and modeling results are described.
- A summary of the findings is then presented along with suggestions on how to improve the analysis.

In general the progression though this evaluation of reference cells using standard methodologies provide limited precision in characterization of reference cells. A Better understand requires a different approach and this study concludes by describing this approach.

2. Experimental setup

A basic understanding of the reference cell guides the experimental setup. The IMT monocrystalline reference solar cell is used in this study as most available reference cells are based on crystalline silicon and have similar behavior. Fig. 1 illustrates the spectral response of an IMT reference cell. Spectral responsivity is proportional to QE times wavelength. For solar cells, the normalized quantum efficiency (QE) is measured and the spectral response is calculated. The normalized quantum efficiency peaks around 600 nm and the spectral response peaks at around 950 nm and goes to zero around 300 nm and above 1249 nm. The uncertainty of the measurement is about 0.2% between 425 nm and 1000 nm at the 95% level of confidence. Outside these limits the uncertainty increases to 10% or more at the extremes.

The spectral response is plotted for two temperatures, 24 °C and 45 °C in Fig. 1. Under short circuit conditions, the spectral response increases as temperature increases especially for wavelengths near the silicon band gap (Hishikawa et al., 2018). This is opposite of what occurs for PV modules where performance decreases as temperature increases. This difference results from PV modules operating at the max power point where voltage is affected by temperature. Reference cells operate close to short circuit current where the voltage is essentially zero and hence is not affected by temperature.

Glazing for reference cells and PV modules are similar and the glazing effects the amount of light transmitted to the solar cell. At normal incidence, light passes through the flat glazing with minimal change. As the angle of incidence increases, the transmission of light through the glazing decreases. The decrease in transmission follows Snell's Law. Glazing used by reference cells, like PV modules, significantly reduces the irradiance entering at large angles-of-incidence (AOI). From AOI of 0° to 45°, the reduction of incident radiation is only about 1% (Marion, 2017). By the time the angle-of-incidence reaches 60°, the reduction is 5% and increases rapidly at larger angles-of-incidence.

Data for this study comes from reference cells, pyranometers, and a spectroradiometer co-located on a one-axis EKO tracker at the National Renewable Energy Laboratory's (NREL) Solar Research Radiation Laboratory (SRRL) in Golden, Colorado. Some data from a similar facility at the University of Oregon Solar Radiation Monitoring Laboratory (UO SRML) in Eugene, Oregon are also examined. Comparisons are made between high quality pyranometer measurements (using a Kipp & Zonen CMP 22) and IMT reference cells on a one-axis tracker. Every five minutes, the EKO WISER spectroradiometers, EKO MS 710 and MS 712, generated spectral data from 350 to 1650 nm (an EKO MS 711 spectroradiometer in Eugene with a range from 300 nm to 1100 nm is also used in this study). The spectroradiometers are calibrated at NREL using a NIST calibrated lamp. This calibration was performed with the spectroradiometer perpendicular to the light source. No dependence on cosine response was measured at the time of calibration. The IMT reference cell was calibrated at NREL against a solar simulator and its

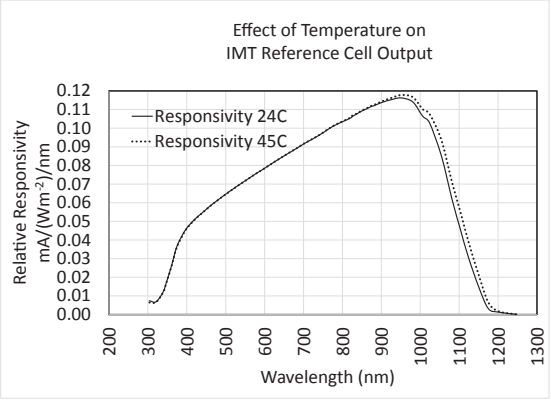

Fig. 1. Relative spectral responsivity of an IMT mono-silicon reference cell. Measurements made at 24 °C and 45 °C under a NIST calibrated lamp.

spectral responsivity was determined. Again, the reference cell's response was measured perpendicular to the light source. The spectral responsivity was measured at three temperatures (24 °C, 35 °C, 45 °C) (see Fig. 1). During the field experiment, the temperature of the reference cell is measured along with its voltage output. The standard deviation of the reference cell responsivity is in the 0.2% range from 400 nm to 1025 nm. Outside this range, the standard deviation of the measured spectral responsivity increases dramatically.

Systematic biases also are associated with the comparison pyranometer. All measurements have uncertainty and many have systematic biases. It is important to identify systematic biases associated with instruments or measurements and indicate how they can influence the analysis or modeling. Therefore it is essential to use a high-quality comparison pyranometer with minimal biases.

The Kipp & Zonen CMP 22 is a Class-A pyranometer and was calibrated using the NREL BORCAL protocol (see BORCAL Report-SW 2017-02 for CMP 22 160430 calibration data). The quoted calibration number and combined uncertainty at the 95% level of confidence is 9.6502 μV/(Wm^{-2}) + 1.4% − 1.8% from 30° to 60°. Because the pyranometer is used continuously, other factors such as soiling add slightly to the uncertainty.

The EKO one-axis tracker is aligned north–south and the platform faces east at sunrise and west at sunset. At solar noon, the solar zenith angle is at minimum, the platform is horizontal. The range of motion of the tracker as used in this experiment at SRRL only allowed the zenith angle of the tracker to rotate from 90° to 0° (as opposed to continuously rotating from 90° to −90° over the day). In order to obtain data in the afternoon, the tracker rotates the azimuthal orientation of the platform by 180° at solar noon. The tracker then rotates the platform until it faces west at sunset. With adaptations, as with the EKO tracker at UO SRML in Eugene, it is also possible to have a continuous rotation from east to west, but this isn't how the SRRL tracker was configured for most of the data used in this experiment.

The spectral responsivity of the IMT reference cell is shown in Fig. 1. The responsivity peaks around 950 nm and is zero above 1250 nm. The spectral responsivity at wavelengths above 950 nm increases as temperature increase. The data used in this study will be available online at a future data on the NREL MIDC website.

The increase in spectral responsivity at higher temperatures for wavelengths greater than 1000 nm is caused by the kinetic energy increase of the electrons. In order for the electron to jump over the gap to the conduction band, the energy of the photon not only has to be sufficient to separate the electron from the atom but it has to impart enough energy so that the electron can jump across the band gap. As the temperature increases, the kinetic energy of the electrons increase. For electrons with energies just below the energy level necessary to jump into the conduction band, the additional kinetic energy may add just enough addition energy to some electrons so that they can jump across the band gap. This kinetic energy *boost* mainly affects electrons separated from atoms by photons with longer wavelengths, in the 1000–1250 nm range, enabling a few more electrons to jump the gap. A more thorough discussion of this effect can be found in (Hishikawa et al., 2018).

3. Calculation of average IMT responsivity

The average responsivity of the IMT reference cell can be calculated using measured spectral data from the spectroradiometer and the temperature of the reference cell (see Eq. (1)). On clear days, the distribution of incident radiation changes throughout the day as path length through the atmosphere changes. Changes in the spectral distribution of the incident radiation changes the average responsivity of the IMT. In Fig. 2, the relative intensity of spectral irradiance versus wavelength is shown at various times for a cloudless day.

To compare the relative change in intensity of the spectral radiation at each wavelength, the spectral intensity is divided by the intensity of the spectral radiation at 500 nm. There is a significant shift in spectral distribution in the early morning (at 6:00 SZA = 86.90°) and late evening hours (at 17:30 SZA = 82.50°). Using information in Table 1 and Fig. 2, it becomes apparent that once the sun reaches a zenith angle below 65° the spectral distribution exhibits minimal differences assuming the aerosol and water vapor content of the atmosphere are fairly constant during the day.

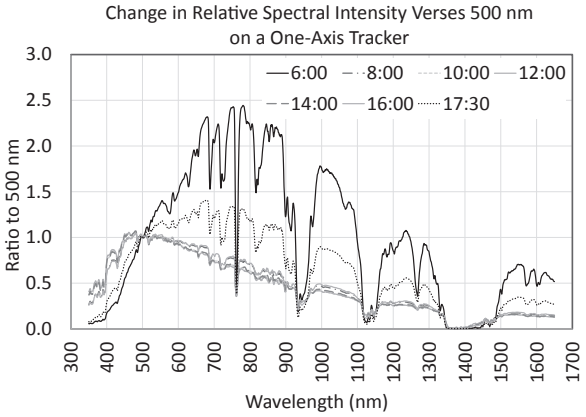

Fig. 2. Relative change in spectral intensity at different times of day of a cloudless day normalized to one at 500 nm on September 13, 2018. Early morning (6:00 – SZA = 87°) and late afternoon (17:30 – SZA = 82.5°) exhibit a dramatic shift in the spectral distribution from distributions during the middle of the day.

The average responsivity of the IMT reference cell is given by Eqs. (1a) and (1b). The spectral responsivity of the reference cell, adjusted for temperature, is multiplied with spectral irradiance of the incident solar radiation. This product is integrated over all wavelengths and divided by the sum of the spectral irradiance over all wavelengths.

$$\overline{R} = \frac{\int_{280nm}^{4000nm} R_\lambda \cdot [1 + T_\lambda \cdot (T_{rc} - 25)] \cdot I_\lambda d\lambda}{\int_{280nm}^{4000nm} I_\lambda d\lambda} \quad (1a)$$

where R_λ is the IMT responsivity at wavelength λ, and I_λ is the intensity of the radiation at wavelength λ, T_λ is the effect of temperature on the responsivity at a given temperature, and T_{rc} is the measured reference cell temperature. The product is integrated over wavelengths from 280 nm to 4000 nm[1]. Since the variables are digital, the integral can be

Table 1
Solar zenith angles for given times on September 13, 2018.

Time	Solar Zenith Angle
6:00	86.90°
8:00	64.32°
10:00	44.76°
12:00	36.15°
14:00	45.62°
16:00	65.50°
17:30	82.50°

[1] The ISO 9060:2018 classifies instrument spectral response by using the spectral range from 280 nm to 4000 nm. About 0.3% of the energy of the solar spectrum comes from wavelengths longer than 4000 nm. There is also downward sky infrared radiation, depending on its temperature. Some radiation from the sky has wavelengths in the 3000 nm to 4000 nm range, but this is very small. To be consistent with the best instruments used to measure solar radiation the reference cells will be compared to the irradiance in the 280–4000 nm range.

evaluated as a sum using Eq. (1b).

$$\overline{R} = \frac{\sum_{280nm}^{4000nm} R_\lambda \cdot [1 + T_\lambda \cdot (T_{rc} - 25)] \cdot I_\lambda}{\sum_{280nm}^{4000nm} I_\lambda} \quad (1b)$$

The wavelength dependence of the temperature coefficient is discussed in (Vignola et al., 2018). In much of the literature, formulas are represented as integrals over the wavelengths and then calculated as sums. In this analysis, the wavelengths for each parameter in Eq. (1b) are one nm apart, but some data have spectral measurements made a different wavelength separations and when that information is use, the interval between wavelengths has to be taken into account.

In Eq. (1b), the wavelengths are summed from 280 nm to 4000 nm. However, the spectral radiometers at SRRL only measure the spectral radiation over a range from 350 nm to 1650 nm. The spectral responsivity of the IMT reference cell is small for λ less than 350 nm and is zero for λ greater than 1250 nms. Calculations using spectral data from the 300–1250 nm range show that neglecting the 300–350 nm contribution only reduces the calculated responsivity by less than 0.02%. Therefore the numerator can be calculated with a fair degree of accuracy with the available spectral data. That cannot be said for the denominator that is the sum of irradiance over 280–4000 nm range.

In Eq. (1b), the denominator calls for the spectral irradiance to be summed from 280 nm to 4000 nm. Spectral measurements run only from 350 nm to 1650 nm. To provide an idea of the bias on the one-axis tracking surface introduced by summing spectral radiation over shorter wavelengths, the spectral radiation is calculated by summing from 350 nm to 1250 nm, 350–1650 nm, and from 280 nm to 4000 nm. Since no spectral measurements are available from 1650 nm to 4000 nm, the broadband measurements from the CMP22 pyranometer can be use to represent the GTI. A comparison of the average responsivity ($\overline{R}$) is calculated using the three different spectral ranges in Fig. 3. The denominator increases as the range of wavelengths used to calculate the incident radiation increases. With the available spectral measurements, the denominator in Eq. (1b) is calculated for the spectral range from 350 nm to 1250 nm and for the spectral range from 350 nm to 1650 nm. A more useful question is, "How does the relative average responsivity changes as the spectral distribution changes over the day, when the denominator includes a greater spectral range?" By looking at the relative change in average responsivity, the influence of the difference weighting of the longer wavelength over the day can be assessed. At what point does the change in spectral distribution of the longer wavelengths start to show non-linear affects. In Fig. 3, the average responsivity of the reference cell is calculated using Eq. (1b) with the denominator calculated for the different spectral ranges. To look at the relative influence of the longer wavelengths, the two shorter ranges were adjusted to equal the results for the full range at the SZA of 47°. (On March 2, the minimum SZA was 47°. Because the IMT responsivity at wavelengths greater than 1250 is zero, the numerator in Eq. (1b) is the same in all three instances. The denominator used to determine the average responsivity increases by including wavelengths from 1250 nm to 1650 nm or 1250 to 4000 nm.

To examine the effect of changing spectral radiation, the relative change in the average spectral responsivity is evaluated rather than examining the absolute change in the average responsivity. In Fig. 3, at a SZA greater than 70°, the shape of the average responsivity ($\overline{R}$) using the spectral values from only 350 nm to 1249 nm start to diverge from the ($\overline{R}$) using the 350–1650 nm range. This indicates that the contributions from 1250 nm to 1650 nm are important to consider at larger zenith angles. For SZA values greater than 80° inclusion of wavelength in the 1650–4000 nm range seem to affect the change of the responsivity ($\overline{R}$) as the spectral distribution shifts. This indicates that for clear skies, the relative change in the denominator from 350 nm to 1650 nm is proportional to changes in the changes in the denominator from 280 nm to 4000 nm for much of the day. Once SZA is greater than 80°, this proportionality breaks down. The split in the broadband curve is related to a leveling issue for the pyranometer and the rotation method used by the one-axis tracker. This will be discussed in greater detail in the discussion Section 8 of the paper.

The data shown in Figs. 3, 5, 6, 7, 8, and 9 have two branches. One in the morning and one in the afternoon. The two branches result from leveling of the instruments and how the tracker is configured. More information on this topic is presented in the Section 6 in which the results are discussed.

4. Clear sky comparison with broadband data

In Sections 4 and 5 the measured and calculated IMT values are compared to the broadband CMP22 pyranometer measurements under clear and totally cloudy skies respectively. The expected IMT output is calculated using the measured spectrum from the spectroradiometer, the temperature of the reference cell, the measured spectral response of the reference cell and the spectral temperature dependence of the reference cell. The absolute responsivity of the reference cell is the numerator in Eq. (1b). The spectroradiometers used in this experiment measures incident radiation from 350 nm to 1650 nm and the broadband pyranometer is sensitive to the wavelength range 280–4000 nm. While the spectral distribution influences the IMT reference cell measurement output other factors such as angle-of-incidence and the temperature also are important. The comparison under clear skies between IMT measurements with reference pyranometer measurements is covered in the section. Figs. 4–7 illustrate characteristics of the relationship between

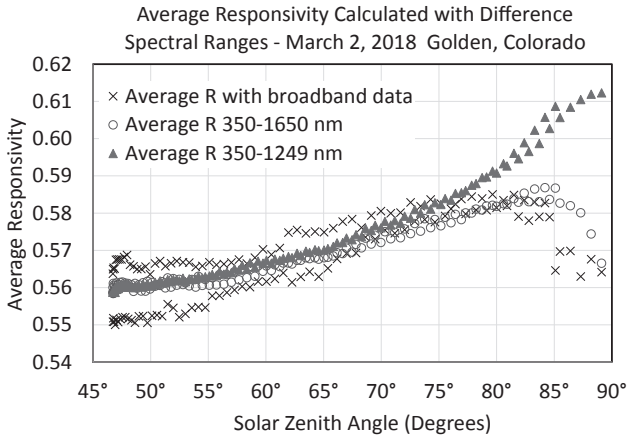

Fig. 3. Comparison of the calculated average responsivity of an IMT reference cell obtained using wavelengths from 350 nm to 1249 nm, with wavelengths from 350 nm to 1650 nm and the use of broadband data for the denominator. The three sets of average R values are set equal at 47°.

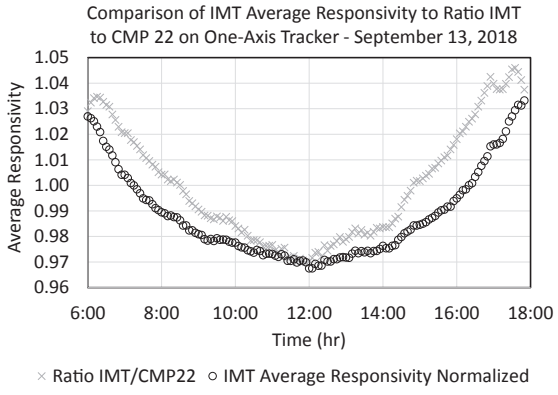

Fig. 4. Ratio of an IMT reference cell to the irradiance measured with a CMP22 pyranometer on a one-axis tracker are shown as x's. The average responsivity from Eq. (1b) is also plotted and the circles.

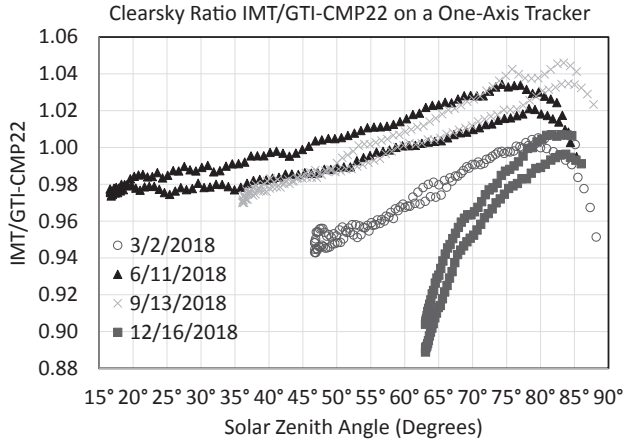

Fig. 5. Ratio of an IMT reference cell to the irradiance measured with a CMP22 pyranometer on a one-axis tracker for different times of year plotted against the solar zenith angle.

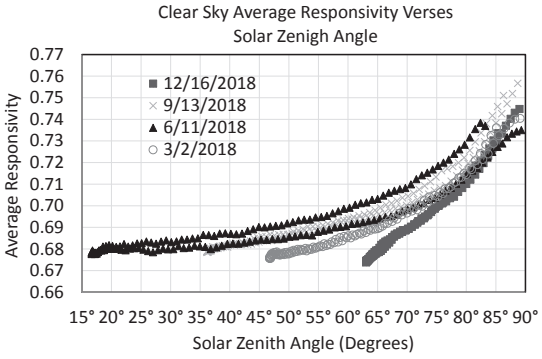

Fig. 6. Plot of IMT reference cell average responsivity plotted against solar zenith angle under clear skies. Reference cell mounted on a one-axis tracker.

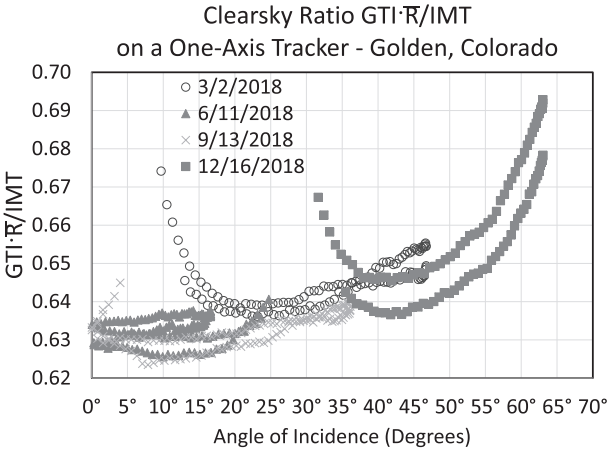

Fig. 7. Ratio of IMT average responsivity multiplied by the GTI measurements from the CMP22 pyranometer and divided by the IMT output on a one-axis tracker under cloudless skies. The ratio is plotted against the AOI.

reference cells and provide a basis for modeling the performance of reference cells.

The postulated relationship between the IMT measurements and broadband measurement is

$$IMT = K \cdot \overline{R}(SZA) \cdot GTI \cdot F(AOI) \tag{2}$$

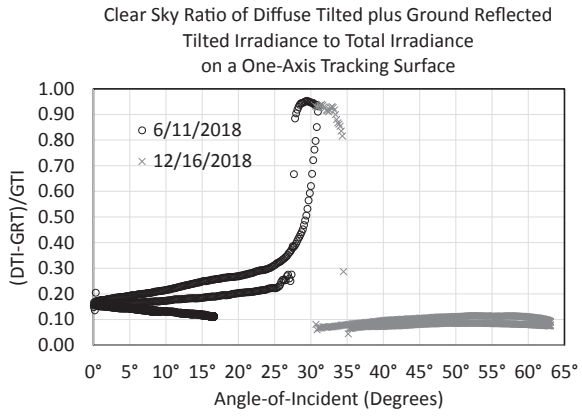

Fig. 8. Clear sky ratio of DTI plus GRT irradiance on a one-axis tracking surface divided by GTI. Data are plotted against the DNI angle of incidence on the one-axis tracker surface. The ratio increases significantly during the early morning hours and late evening hours (*AOI* of 25° – 30° for summer and 30° – 35° for winter). These periods are when DTI and GRT contribute significantly to the GTI. Data from Golden, Colorado.

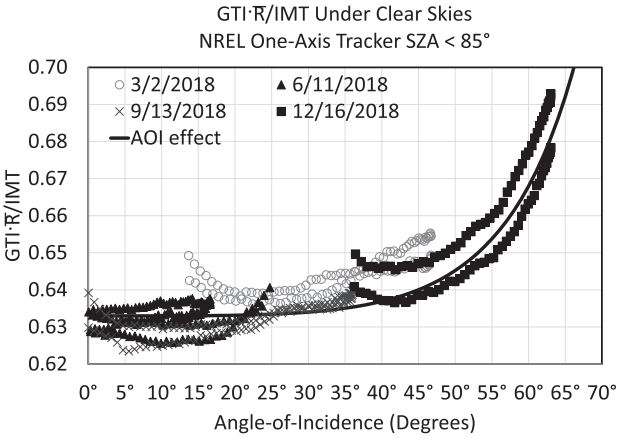

Fig. 9. Same as Fig. 7 with the data limited to SZA less than 85°. The AOI effect is plotted and shows that it is important to consider when AOI is greater than 35°.

where the average responsivity $\overline{R}(SZA)$ is the relative average responsivity determined via Eq. (1), *GTI* is the broadband total irradiance on the one-axis tracking surface, *F(AOI)* is the angle-of-incidence function that accounts for the non-linear *AOI* characteristics of the IMT glazing, and *K* is similar to a responsivity that relates the measured current or voltage to the total irradiance. Because this relationship is not exact, other factors can be can also contribute to the *K* value such as the scale factor relating the summed spectral irradiance over the range for which data are available and adjustments to calibration values obtained at different angles-of-incidence.

A simple method to explore the relationship between the IMT reference cell and broadband measurements is illustrated in Fig. 4 that plots the ratio of IMT measurements to the GTI values obtained by the reference pyranometer. The gray x's shown in Fig. 4 are the ratio of the IMT reference cell output to the irradiance from a CMP22 pyranometer. A similar curve can be obtained by plotting the average responsivity obtain from Eq. (1b). In this example the circles in Fig. 4 are the average responsivity multiplied by a constant chosen so that the two curves match at noon. The data are obtained under clear sky periods on September 13, 2018. The two curves are similar in shape and varies from about 0.97 at solar noon to about 1.04 in the early morning and late afternoon.

If the *AOI* effect was minimal, one would expect the two curves to align. While there is some agreement between the curves, the *AOI* effects influence the comparisons to a measurable degree.

By choosing a variety of clear days over the year the various spectral, angle-of-incidence, and temperature effects that influence the IMT measurements are examined. Four days with clear skies at different times of year were selected.

The ratio of the IMT measurements to the GTI measurements from the CMP22 pyranometer is plotted against the solar zenith angle in Fig. 5. Both instruments are co-located on the one-axis tracker. The IMT values differ from the CMP22 measurements by up to 10% depending on the time of year and the solar zenith angle. The CMP22 has a small uncertainty ~ 2.5% or smaller under a wide variety of weather condition at the 95% level of confidence. The uncertainty under clear sky conditions is likely to be better. The pyranometer, with a reliable cosine response, is minimally affected by ambient temperature, and has a uniform wavelength response over much of the spectral range. The CMP22 is therefore considered the reference against which to compare the IMT irradiance values. The spectral, *AOI, and* temperature biases of the reference cell, cause much of the differences seen in the plot.

Several factors influence the comparison between reference GTI pyranometer measurements and IMT reference cell's measurements. Some of these factors can be seen by the different characteristics of the curves in Fig. 5 and Fig. 6. The *F(AOI)* effects are a significant contributor to the differences. The value *K* should be the same for all datasets. Neglected in all analysis is the contribution from spectral irradiance in the 280–350 nm range. This contribution in this range is be between 0.0 and 0.02% as compared to calculations in the 350–1250 nm range because the spectral responsivity of the *IMT* is small at these low wavelengths as is the intensity of solar radiation.

A clearer way to examine the *AOI* dependence is to plot the ratio of GTI divided by the IMT values times $\overline{R}$ from Eq. (1b) against the *AOI* for different clear days through the year. This is done for the same clear sky days used in Figs. 5 and 6. The average responsivity of the IMT reference cell times GTI and divided by the IMT measurements is shown in Fig. 7. The same R_λ and T_λ were used for all days and the I_λ and T_{rc} were measured on the specific days examined.

The functions in Eq. (2) can be rearranged to look at *F(AOI)*

$$1/(F(AOI)\cdot K) = GTI\cdot\overline{R}(SZA)/IMT. \tag{3}$$

Plotting the right hand side of Eq. (3) yields an estimate of the inverse of *F(AOI)* times *K* as shown in Fig. 7 which is plotted against *AOI*.

A majority of data in Fig. 7 fall along a bottom curve. However, all days exhibit spikes. Closer examination of the spikes show these data occur in the early morning or late afternoon. Data obtained during the early morning hours and before sunset are atypical of the data obtained during the rest of the day (see Fig. 8). This results from the different fields of view of the instruments mounted on a one-axis tracker with respect to obstructions near the horizon and a relative increase in the diffuse tilted irradiance (DTI) and the ground reflected tilted irradiance (GTR). The mountains west of the site in Golden, Colorado blocks the horizon in the late afternoon. Also there are obstructions and different ground reflectivities seen in the morning. The data are plotted against the angle-of-incidence of the DNI on the tracker surface. Near dawn or sunset on a one-axis tracker in June (circles in Fig. 8) the SZA is near 90° with an angle-of-incidence near 30°. In December (x's in Fig. 8) when the SZA is near 90° the angle-of-incidence is again near 30°. In both cases, the ratio of DTI plus GRT to GTI rapidly increases towards 1 near sunrise and sunset.

Fig. 9 is a plot of the same data as shown in Fig. 7 with values obtained when the solar zenith angle is greater than 85° eliminated. This removes many of the extreme points see in Fig. 7. The solid black line added to Fig. 9 is the inverse *F(AOI)* multiplied by 0.663 using the angle-of-incidence model found in Eq. (6) of Marion, 2017. This part of the model in Marion, 2017 is for irradiance of a known direction and is based on Snell's Law and Fresnel equations. The value 0.633 was obtained by fitting the curve to the average value when *AOI* is zero. In Fig. 9, *K* is 1/0.633 or 1.58. The data in Fig. 9 indicates that to within 1% to 2%, spectral, temperature, and *AOI* effects account for most of the difference between the IMT reference cell measurements and the pyranometer measurements.

An exact calculation for the *F(AOI)* factor includes the DTI and GRT contributions, values that have to be integrated over all directions of the incident diffuse and reflected irradiance. Since *F(AOI)* changes by less than 1% for *AOI* from 0° to 45°, see Fig. 9, and the DTI and GRT have minimal contributions GTI under clear skies (see Eq. (4)), the *F(AOI)* effect on GTI will be modeled with *AOI* determined as if all irradiance is coming directly from the sun.

$$GTI = DTI + GTR + DNI\cdot\cos(AOI) \tag{4}$$

The assumption that *F(AOI)* can be determined by assuming all incident radiation is coming directly from the sun during cloudless periods is based on the relative contributions of the DTI and GRT irradiance only contributes 20% or less and any difference between the GTI modeled from the DNI F(AOI) function and inclusion of the DTI and GRT AOI effects are on the order of 1%. A discussion of the DTI and GRT irradiance is given in Section 5 when measurements under cloudy skies are evaluated.

5. Comparisons under totally cloudy skies

The relationship between reference cell and pyranometer is more complex under cloudy skies because GTI has much larger contributions from DTI and GRT irradiances percentage wise. In addition, spectral measurements used in this study are only done once every 5-minutes and occur over only at the top of that minute. The GTI readings are scanned every three seconds and averaged over the minute. Only the minutes when the spectral measurements were made are used. Since GTI can vary significantly over a minute, the spectral measurements may not accurately represent the average values during the minute, especially if the irradiance is changing rapidly. To provide a more stable comparison, totally cloudy skies when the DNI is near zero are examined. Therefore GTI consists entirely of the sum of DTI and GRT.

A plot of average IMT responsivity under totally cloudy skies at four different times during the year are shown in Fig. 10. Similar data for clear skies is plotted in Fig. 6. While no clear pattern is apparent, the overall average IMT responsivity is about 0.65 ± 0.03 and exhibits about a 5% standard deviation. Since the DTI and GRT irradiance come from all areas visible to the instrument, there is minimal preferential direction and a pattern is not expected.

Under clear skies, as shown in Fig. 9, the average responsivity is

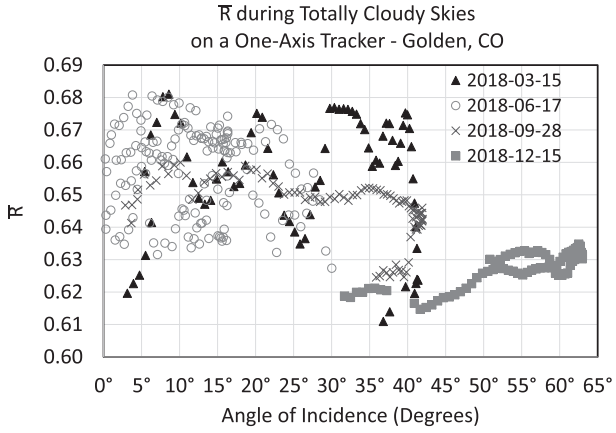

Fig. 10. Average responsivity *R* of an IMT reference cell under totally cloudy skies. For comparison with earlier plots, the axis is the *AOI* of the DNI irradiance.

multiplied by GTI and divided by the IMT measurement. This results in a clear pattern that matched the *F(AOI)* factor for DNI irradiance. The average responsivity under cloudy skies was again multiplied by GTI and divided by the IMT measurement as shown in Fig. 11. Under totally cloudy skies there should be no dependence on *AOI* as DTI and GRT irradiance come from a wide variety of angles. Included in Fig. 11 is the *F(AOI)* factor for DNI irradiance from Eq. (3). The standard deviation between the measured values and the modeled average responsivity and the ratio between IMT and GTI effect is about ±0.02 or about 3%. While there is considerable scatter in Fig. 11 there is about a 40% decrease in the standard deviation from the data in Fig. 10.

Using models in Marion (2017), the reduction of irradiance passing through standard glass glazing can be calculated for the three components of diffuse radiation and ground reflected radiation. The three diffuse components, (Perez et al., 1990), are the circumsolar diffuse, horizon brightening, and the diffuse radiation from the rest of the sky. The Perez model divides the diffuse irradiance into three components, brightening around the sun (circumsolar), horizon brightening, and a distribution across the sky proportional to $(1 + \cos(T))/2$ where T is the tilt of the surface at a given instant. For a one-axis tracking surface, T varies with time. The GRT can be model as proportional to $GHI \cdot \rho \cdot (1 - \cos(T))/2$ where ρ is the ground reflectance and T is still the tilt of the surface. The model derived in Marion (2017) uses the breakdown by Perez and obtains the average transmission by integrating and averaging over all directions of the irradiance on the tilted surface using the Perez et al. (1990) breakdown. The reduction for the diffuse components and ground reflected irradiance are shown in Fig. 12 where F_{Sky} is the reduction from the background sky, F_{Hor} is the reduction associated with horizon brightening, and F_{GRT} is the reduction of ground reflected irradiance. The *F(AOI)* for the circumsolar diffuse component is treated the same as the *F(AOI)* for the DNI irradiance on the one-axis tracking surface. Values in Fig. 12 are plotted against the tilt of the one-axis tracking surface that goes from 90° east facing in the morning to horizontal, 0°, at solar noon, to 90° west facing at sunset. The plots shown in Fig. 12 will vary slightly for glazings with different transmission characteristics.

If the diffuse and ground reflected transmission values are multiplied by 1/K value of 0.633 and shown in Fig. 11 they would yield values of 0.65 or slightly higher. The exact value is dependent on how the diffuse components and ground reflected values are determined. The uncertainty of the input data and the methodology used to evaluate the data, inhibits a detailed evaluation of the transmission model for the diffuse and ground reflected components (see Section 6).

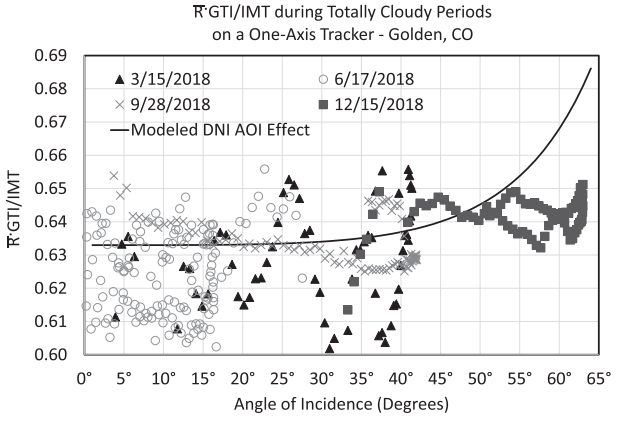

Fig. 11. Average responsivity of an IMT reference cell times GTI/IMT during totally cloudy skies. Included is the inverse of *K·F(AOI)* with the same values used in Fig. 9.

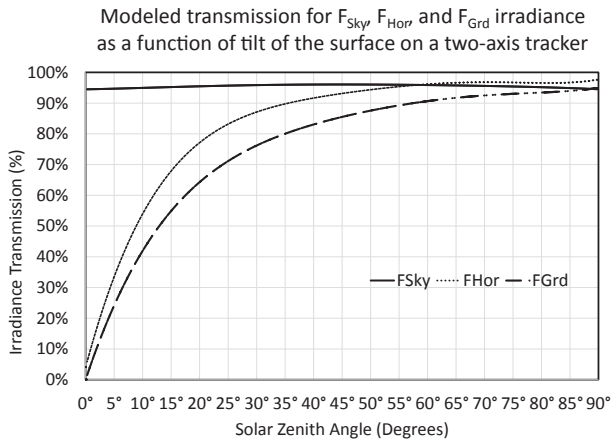

Fig. 12. Model transmission of diffuse sky and horizon brightening irradiance and ground reflected irradiance plotted against the tilt of the one-axis tracking surface.

6. Discussion of results

Having reference cells collocated with a reference pyranometer and spectral radiometers covering a 350–1650 nm range provides a unique opportunity to examine the characteristics of reference cells. While it may be possible to emulate the pyranometer output to the 2% level under clear skies, spectral data from a spectroradiometer or an accurate spectral model are necessary to directly relate the IMT output to the GTI (total) on the one-axis tracking surface. Once the behavior of reference cells is accurately characterized, spectral models will be needed for general use of the findings. Using spectral data enables testing and/or developing theoretical models of the differences between broadband reference pyranometer measurements and reference cell measurements. In addition, the results obtained here should be applicable to PV modules, using model spectrums, because they behave much like reference cells.

As shown in Fig. 5, the difference between the data and the modeled estimate varies over the day. The difference is greatest at large SZA where the path length through the atmosphere significantly affects the spectral distribution. Therefore, one would expect the greatest spectral effects to be in the early morning and late afternoon hours. This is borne out by the modeled results.

There is a slight asymmetry between the morning estimated ratios and the afternoon estimated ratios. One might assume that this difference is the result of the temperature dependence of reference cell output. However, the temperature effects are small and have already been taken into account. Also, this does not explain the two branches seen in the each day's data that are shown in Figs. 7 and 9. The branches result from a jump in output at solar noon that cannot be explained by slow temperature changes.

Fig. 14 illustrates the output from the CMP22, the 520 nm data from an EKO spectroradiometer, and the IMT reference cell on a clear day in December. All three instruments are on an EKO one-axis tracker. The tracker is configured so that the platform upon which the instruments are mounted rotates 180° at solar noon enabling the platform to rotate from east to west during the day. This rotation seems to have little effect on the IMT reference cell, but data from the pyranometer exhibits a 1.5% decrease and the EKO spectroradiometer data exhibits a 1.5% increase at solar noon. Other months and other pyranometers also exhibit this effect, although not as much as seen in December. The platform is horizontal during this rotation, so north–south alignment of the tracker is not the cause. One likely cause of this jump is if the instrument is tilted 0.3° to the south. Then when it is rotated 180° it would be tilted 0.3° to the north. During clear periods, global irradiance is mostly dependent upon the direct normal irradiance times the cosine of the solar zenith. In

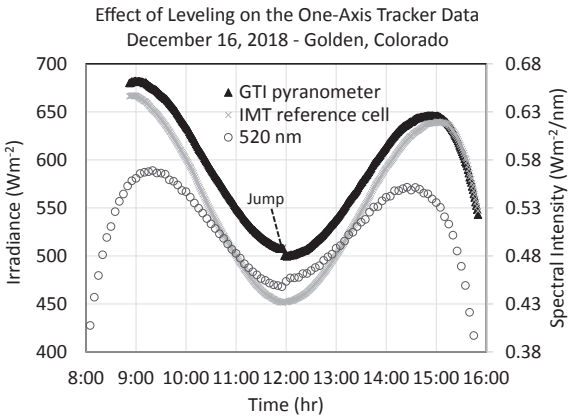

Fig. 13. Measurements from a CMP 22 pyranometer, an IMT reference cell, and an EKO spectroradiometer on a one-axis tracker. The platform on the EKO tracker rotates 180° at solar noon.

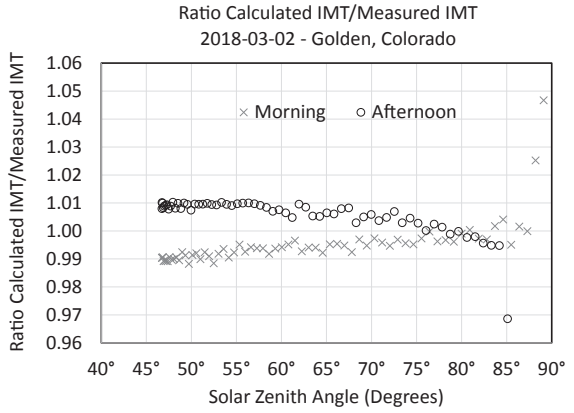

Fig. 14. Comparison of the modeled verse the modeled IMT values on a clear day - March 3, 2018. The morning values are x's and the afternoon values are circles. In this example, the noonday values have the smallest solar zenith angles while having the largest angles-of-incidence.

December, when the solar zenith angle is about 67° in Golden, this slight tilt would result in about a 1.5% decrease in the projected direct normal irradiance projected onto the pyranometer at solar noon. The spectroradiometer also seem to be tilted by about 0.3°, but to the north. Since the pyranometer acts as a reference measurement and the spectral data are used to determine the average responsivity of the IMT reference cell, any analysis needs to take the effect of leveling into consideration especially at large solar zenith angle. The problem with this leveling issue shows clearly in clearly in Fig. 5, Fig. 7, and Fig. 9 and this bias added to the uncertainty to the evaluation of the measurements. This is an excellent example of the need to examine all the measurements that go into any final analysis and conclusion.

As mentioned earlier, the uncertainty with the Class-A broadband pyranometer measurements is on the order of ±2.5%. Relative uncertainty can be much less, but the instrument must be well characterized. For example, the directional uncertainty of a CMP22 pyranometer is less than 5 W/m^2. While small, these and other uncertainties have to be incorporated into any uncertainty quoted for the final analysis.

Not covered in this discussion is the uncertainties in the IMT measurements. The IMT calibration value was determined in the lab and not in the field. The calibrations in the lab were done with the reference cell perpendicular to the incident reference lamp. If it was determined in the field, the value would be dependent upon the spectral distribution of the incident radiation at the time of calibration and the angle-of-incidence. Because of angle-of-incident affects, the field responsivity of the reference cell measured at 45° is about 1% higher than that at 0° as it was measured in the laboratory (see the plot of *F(AOI)* in Fig. 9).

The difference in the temperature dependence the reference cell and the reference pyranometer affect the results in this comparison. The temperature dependence of the CMP 22 pyranometer is less than 0.5% over a range of ambient temperature from −20 °C to 50 °C. The reference cell has a larger temperature dependence of about 0.08% per °C change or about 4% over a 50 °C change in the temperature of the reference cell. The reference cell temperature dependence varies with the spectral distribution of the incident radiation and the spectral data can be used to estimate the effect of temperature on the reference cell output. Without spectral data, an average temperature adjustment can be made. Under clear skies, the temperature of the reference cell is lowest in the morning and evening and highest in the early afternoon. The difference between the spectrally adjusted temperature and the average, spectrally independent, temperature affect is on the order of 1% at a reference cell temperature of 50 °C and the results match at 25 °C

The effect of the angle-of-incident is the other factor that influences the ratio of the reference cell to the reference pyranometer. For the one-axis tracker in mid-September, the angle of incident changes from about 30° at noon to 0° just after sunrise and just before sunset. A simple model of the DNI angle-of-incidence affect (Marion, 2017) is illustrated in Fig. 9. This model is based on the physics of light transmission through glass and is very rigorous at small angles of incidence. At larger angles, spectral effects make it difficult to test the model. Under clear skies, this angle-of-incidence model is used for both direct normal and diffuse irradiance incident upon the surface.

If the spectral, temperature, and angle of incident effects are taken into account, the cosine response characteristics of the Class-A pyranometer and the spectroradiometer still need to be considered. The CMP 22 has an angular response of 0.5% or better at 1000 W/m^2. The angular response of the spectroradiometer is small but the number of field tests is limited.

An alternate method to evaluate the performance of the reference cell is to look at how well the spectral data and modeling can duplicate the IMT output. Up to now, the comparisons presented calculate the denominator in Eq. (1a) by summing over the measured spectral data in the 350–1650 nm range. This serves well for relative comparisons. To remove bias and uncertainty associated with in the assumption that the sum of spectral irradiance data from 350 nm to 1650 nm is proportional to the sum of the spectral radiation from 280 nm to 4000 nm, the GTI measurements of the reference pyranometer will be used as the measure of the total irradiance in the 280–4000 nm range. While all pyranometer measurements have some bias and uncertainty, the measurement from a reference pyranometer is certainly as accurate of the sum of spectral data from 280 nm to 4000 nm using a spectral model. The relationship between the IMT output and the model estimates of the reference cell output are actually simplified by using the GTI measurement for the sum of radiation over all wavelengths. What happens is that the GTI used as the sum of radiation over all wavelengths cancels with the GTI in the numerator in Eq. (2). The result is Eq. (5).

$$IMT = F(AOI)\cdot K\cdot \int_{280nm}^{4000nm} R_\lambda \cdot \left[1 + T_\lambda \cdot \left(T_{referencecell} - 25\right)\right]\cdot I_\lambda \cdot d\lambda \qquad (5)$$

While the model in Eq. (5) uses all wavelengths, the spectral responsivity of the reference cell (R_λ) is zero below 300 nm and above 1250 nm, the spectral measurements in the 350–1650 nm range cover almost all of the spectral range over which the reference cell generates a current. Since the responsivity of reference cells is so low below 350 nm, the contributions in the 300–350 nm spectral range contribute little to the IMT output (~0.1%). Therefore, the model can be tested with measurements of the reference cell output (*IMT*) and temperature (T_{rc}) and the intensity of the spectral radiation (I_λ). *F(AOI), K,* R_λ, and T_λ are the model parameters.

The ratio of the calculated IMT output to the measured IMT output is used to evaluate the model shown in Eq. (5). If the assumptions for modeling the reference cell are valid, then there should be a linear relationship between calculated output of the reference cell using spectral irradiance data and the measurement of the reference cell. The parameters R_λ, and T_λ values are fixed and I_λ and T_{rc} are measured. The *F (AOI)* is calculated using the Marion, 2017 model and *K* is 1.718. This value of *K* differs by about 8% from the value used in the earlier examples such as the data shown in Fig. 9. This difference relates to the different methodology to obtain the average responsivity. In the earlier example, the sum of the spectral data from 350 nm to 1650 nm was used to calculate the total spectral irradiance shown in the denominator of Eq. (1). In Eq. (3), the average responsivity obtained from Eq. (1b), used the sum of spectral irradiance from 350 nm to 1650 nm and this average is multiplied by the GTI and divided by the output of the IMT in the earlier analysis.

The sum over all wavelengths is equivalent to the total irradiance on the surface. Since pyranometers are designed to measure the GTI, the sum over all wavelengths should equal the sum of spectral irradiance over all wavelengths to with the uncertainty of the measurements. Since Class-A pyranometers are sensitive spectral radiation over the whole 280–4000 nm, the total measured GTI should be greater than the sum of spectral measurements from the 350 nm to 1650 nm spectral range. For March 2, 2018, the difference between pyranometer measurements and the sum over the partial range is ~9%. This accounts for the difference between the value of *K* used for the analysis in Fig. 14 and the value of *K* used in the earlier analysis. For the data studied, it is a good indication that sum of spectral data from 350 nm to 1650 nm is proportional to the sum from 280 nm to 4000 nm over the day.

When *F(AOI)* is calculated using the angle-of-incidence to the tracking surface. This is an approximation as diffuse and reflected sunlight can come from many directions. However, as shown in Fig. 8, the diffuse and ground reflected components are small compared to the DNI incident on the tracker's surface. As mentioned earlier, the DHI and ground reflected irradiance striking the surface with an *AOI* less than 40° have an angle-of-incidence effect of less than 5%. This assumption and the use of spectral and temperature responsivity measured under laboratory conditions enable a direct comparing the reference cell measurements and the calculated value using spectral data. In Fig. 13, the ratio of the calculated IMT values to the IMT measurement is used to evaluate any dependence on solar zenith angle. This ratio can also be plotted against angle-of-incidence or other variables.

The ratio shown in Fig. 14 is not a straight line but consists of two sections. One section in the morning and one in the afternoon. At solar noon, around 47°, a marked shift is observed. The jump seen at solar noon is the result of a slight tilt of the spectroradiometer to the north in the morning (see discussion for Fig. 11). As has been discussed, as the tracker platform rotates 180° at solar noon, the reference cell has a slight tilt to the north in the afternoon. The spectroradiometer shows no change around solar noon (Fig. 11). This tilt results in the split in the data shown in Fig. 14. Given the uncertainties in the measurements and the assumptions made, this comparison provides confidence in the methodology used.

As a companion experiment, a one-axis tracker with a spectroradiometer and reference cells was installed in Eugene, Oregon. The tracker in Eugene rotates continuously through the day and does not perform this 180° rotation at solar noon. The ratio of the calculated reference cell output to measured reference cell output is shown for data from Eugene in Fig. 15. The parameters used for the calculated reference cell output was the same as for the data from Golden, Colorado except that a *K* of 1.756 was used. For the July 20, 2019 data the relationship between the calculated and measured reference cell output seem fairly constant throughout the day. It is expected that each reference cell will have a slightly different calibration factor as there is a slight difference in reference cell performance and the shunt resistance used to produce the voltage output will vary slightly. For the November 1 and 2, 2019 data,

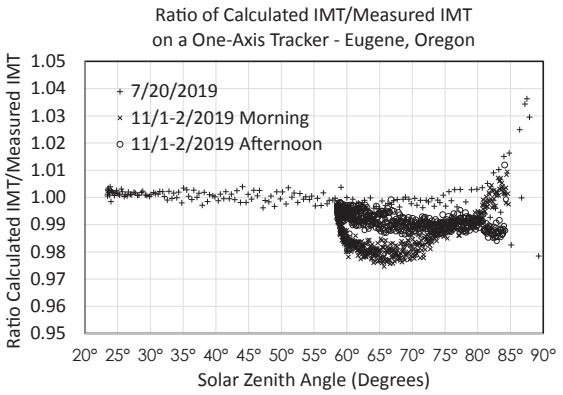

Fig. 15. Comparison of the modeled verse the modeled IMT values on clear days in Eugene, Oregon. The mornings of November 1 and 2, 2019 values are marked with x's and the afternoons are shown as circles. The data for July 20, 2019 are shown as +'s.

the morning and afternoon data differ. The data for the morning and afternoon agree at solar noon, as would be expected from a one-axis tracking system that rotates continuously. It is unclear why the morning and afternoon data are different. Both days were bright cold sunny days and temperatures were near 0 °C both mornings.

The range of the spectral data in Eugene was from 300 nm to 1100 nm. Spectral measurements above 1100 nm were not available. It is possible to estimate the effect on the average responsivity of omitting the spectral range from 1100 nm to 1249 nm by using the Golden, Colorado data. The ratio of the calculated IMT output using 350–1100 nm spectral data was compared to the same calculated IMT result using the 350–1249 nm range. The results are shown in Fig. 16. By omitting the spectral data between 1100 nm and 1249 nm the calculated IMT output was reduced by up to 1.3%, depending on the solar zenith angle. This is an example of how systematic biases can enter to analysis. Still a 2% difference represents a fairly good agreement between a calculated output and a measured output.

7. Next steps

Evaluation of the initial data used to test reference cells and photodiode-based pyranometers on a one-axis tracker suggest several changes in the experimental methodology employed for the testing. The most important is to switch to a tracker mode when the tracking surface follows a continuous arc from sunrise to sunset without rotating 180° at solar noon. This method works well for energy production from photovoltaic panels, but is susceptible to leveling problems when examining

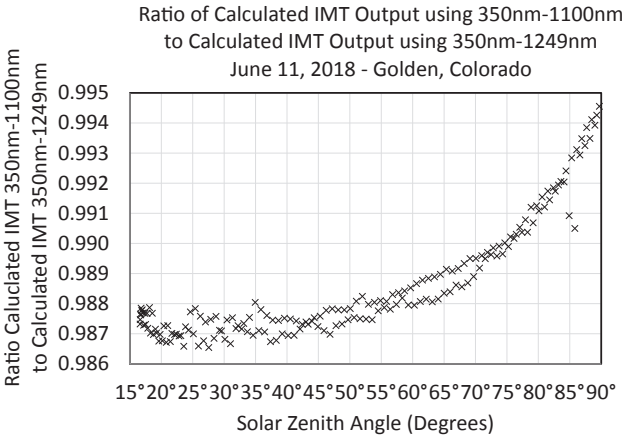

Fig. 16. Ratio of calculated IMT output using 350 nm to 1100 nm range to calculated IMT output using 350 nm to 1249 nm range.

incident radiation. Leveling of instruments is still important even if this would not be so apparent on a continuously rotating surface. It is difficult to level instrument precisely, but even a slight alignment problem can become apparent when the angle-of-incidence becomes large.

Before speculating on possible causes of the difference between modeled and measure results, more data should be examined in detail and against a variety of environmental parameters. A similar experiment is underway in Eugene, Oregon with a spectroradiometer that measures irradiance from 300 nm to 1100 nm. Tests have shown that omitting the 1100–1249 nm range can reduce the calculate IMT output by up to 1.3%. This factor has to be taken into account when using the data from The UO SRML station. By using the NREL's SRRL station data, this issue can be addressed to a reasonable degree. The value of have tests at two different stations is very important to identify unforeseen factors. In addition the SRRL data can always be analyzed in the 350–1100 nm range to evaluate differences caused by the site.

Modeling irradiance, let alone spectral irradiance on a tilted or one-axis tracking surface has much larger uncertainties. While calculating the average responsivity on a horizontal where the full 280–4000 nm spectral distribution can be modeled, it should be possible to identify any significant spectral effects by using a more limited spectral range of 350–1650 nm or even just to 350–1050 nm. For any surface that experiences significant irradiance at angles other than normal incidence, a model of the angle-of-incident effects is needed. The AOI model of Marion, 2017, seems to work well, but more thorough testing over a variety of circumstance is need for a better estimate of the uncertainties.

To minimize the angle-of-incidents effects and to concentrate on validating the spectral and temperature modeling, experiments on a two-axis tracker are recommended. Angle of incidents effects will always be present because the diffuse and ground reflected irradiance also contribute to the total irradiance on a tilted surface. However, the direct normal irradiance is the major contributor to the irradiance for an instrument mounted on a two-axis tracking surface. The diffuse and ground reflected irradiance should be minimal for days with clear skies when there is no highly reflective surfaces, like snow, in the foreground. The angle-of-incident affects are less than 1% for diffuse and ground reflected irradiance with AOI less than 45°. This should further reduce AOI problems caused by diffuse and ground reflected irradiance. As the surface becomes more vertical ground reflected and diffuse irradiance can contribute more to the total tilted irradiance. With data from instruments on a two-axis tracker, the leveling and pointing errors are small. In addition both the spectroradiometers and the reference cells are calibrated at normal incidence. Using Borcal calibration results it should be possible to get high quality estimates of the reference pyranometer at normal incidence. This further reduces the uncertainties and enables a more precise determinate if the simple model for the reference cell performance is reliable.

8. Significance of findings

Reference cells are used to monitor and evaluate PV system performance in the field. To compare results from studies using reference cells to those using broadband pyranometers it is necessary to characterize the reference cells and to understand any biases in the data generated using reference cells. The finding from this study shows that changes in spectral irradiance are a major source of bias. In addition, angle-of-incidence effects also significantly influence the output of reference cells. While temperature effects were included in this study, they are much smaller than the biases related to the spectral distribution of incident radiation and angle-of-incidence effects. Characterizing and quantifying these biases enables comparisons with tests and evaluations of PV systems done with high quality broadband pyranometers. In addition, the knowledge gained quantifying environment effects on reference cell measurements can be applied to the evaluation and modeling of PV systems because their spectral and angle-of-incident sensitivities are very similar to those of photovoltaic modules.

Modeling the performance of reference cells is based in large part on determining the average spectral responsivity of the reference cell. The reference cell is sensitive to irradiance in the 300–1250 nm range. However, determining the average responsivity requires the knowledge of the spectral irradiance in the 300–4000 nm range, the total irradiance on the surface. The difficulty of measuring or modeling the spectral radiation over the whole range can be addressed by using the total irradiance on the surface measured with a high-quality pyranometer. Unfortunately this approach eliminates the dependence on the GTI – total irradiance on the surface (see Eq. (5)). The advantage of using the broadband irradiance measured with a high-quality pyranometer is that other factors such as spectral dependence and angle-of-incident effects can be studied in greater detail. This is a subject for further research.

Declaration of Competing Interest

The authors declare that they have no known competing financial interests or personal relationships that could have appeared to influence the work reported in this paper.

Acknowledgments

The UO Solar Radiation Monitoring Laboratory would like to thank the National Renewable Energy Laboratory as well as the Bonneville Power Administration, Energy Trust of Oregon, and Portland General Electric for the support that makes this work possible. This work was authored in part by Alliance for Sustainable Energy, LLC, the manager and operator of the National Renewable Energy Laboratory for the U.S. Department of Energy (DOE) under Contract No. DE-AC36-08GO28308. via the U.S. Department of Energy under Contract No. DE-AC36-08GO28308. Funding provided by U.S. Department of Energy Office of Energy Efficiency and Renewable Energy Solar Energy Technologies Office. The views expressed in the article do not necessarily represent the views of the DOE or the U.S. Government. The U.S. Government retains and the publisher, by accepting the article for publication, acknowledges that the U.S. Government retains a nonexclusive, paid-up, irrevocable, worldwide license to publish or reproduce the published form of this work, or allow others to do so, for U.S. Government purposes.

References

Broadband Outdoor Radiometer Calibration Shortwave – BORCAL-SW 2017-02 customer Mike Dooraghi, calibration date 05/24/2017.

Habte, Aron, Sengupta, Manajit, Xie, Yu, Dooraghi, Mike, Reda, Ibrahim, Driesse, Anton, Gueymard, Christian, Wilbert, Stefan, Vignola, Frank, 2018. Developing a Framework for Reference Cell Standards for PV Resource Applications. Golden, CO: National Renewable Energy Laboratory. NREL/TP-5D00-72599.

Hishikawa, Yoshihiro, Yoshita, Masahiro, Ohshima, Hironori, Yamagoe, Kengo, Shimura, Haruya, Sasaki, Ayumi, Ueda, Takashi, 2018. Temperature dependence of the short circuit current and spectral responsivity of various kinds of crystalline silicon photovoltaic devices. Jpn. J. Appl. Phys. 57, 08RG17.

Marion, B., 2017. Numerical method for angle-of-incidence correction factors for diffuse radiation incident photovoltaic modules. Sol. Energy 147, 344–348.

Meydbray, J., Emery, Keith, Kurtz, Sarah, 2012. Pyranometers, reference cells: the difference, PV Magazine, April, 2012.

Perez, R., Ineichen, P., Seals, R., Michalsky, J., 1990. Modeling daylight availability and irradiance components from direct and global irradiance. Sol. Energy 44, 271–289.

Vignola, F., Chiu, Chun-Yu, Peterson, Josh, Dooraghi, Michael, Sengupta, Manajit, 2017. Comparison and Analysis of Instruments Measuring Plane-of-Array Irradiance for One-Axis Tracking PV Systems. In: IEEE-PVSC-44.

Vignola, F., Peterson, Josh, Chiu, Chun-Yu, Dooraghi, Michael, Sengupta, Manajit, Mavromatakis, Fotis, 2017. In: Comparison of Pyranometers and Reference Cells on Fixed and One-Axis Tracking Surfaces, American Solar Energy Society Solar Conference.

Vignola, F., Chiu, Chun-Yu, Peterson, Josh, Dooraghi, Michael, Sengupta, Manajit, 2018. Evaluation of Photodiode-based Pyranometers and Reference Solar Cells on a Two-Axis Tracking System. In: IEEE-PVSC – 45.

Vignola, F., Peterson, J., Kessler, R., Sandhu, V., Habte, A., Sengupta, M., 2019. Improved Field Evaluation of Reference Cell Using Spectral Measurements. In: 2019 IEEE 46th Photovoltaic Specialists Conference (PVSC), Chicago, IL, USA, 2019, pp. 3156–3163. https://doi.org/10.1109/PVSC40753.2019.8980915.